Technical Report:

Radiometric Calibration of Visible-channel Meteorological Imagers by Reference Against the Moon

Dr. Thomas C. Stone
USGS Astrogeology Science Center
Lunar Calibration Project Scientist

31 December 2013

Abstract

Developing Climate Data Records (CDRs) from the operational observation data of meteorological satellites requires that the sensors which produced the data be calibrated consistently over time and between instruments. Because the visible-channel imagers on meteorological satellites typically were not equipped with on-board radiometric calibration capabilities, external reference sources and special methods must be employed to realize such calibrations. The established technique of using the Moon as a source of spectral irradiance has been applied to lunar images found in the archives of operational satellite data. Analysis of comparisons between the measurements from these images against the reference standard provided by the USGS lunar calibration system has produced expressions to convert raw image data to radiances in a consistent manner. This report presents these radiance conversion expressions, and documents the procedures used to develop them. The analysis was carried out and this document was prepared for the Climate Data Records Program at the NOAA National Climatic Data Center under Interagency Agreement #NA11AANEG0241.

1 Overview and Purpose

The NOAA National Climatic Data Center is tasked with creating and distributing long-term global Climate Data Records (CDRs) with the quality necessary for assessing global climate variability and change. To develop CDRs spanning decade-length time scales necessarily involves assimilation of operational datasets from observing systems on multiple satellites. It has long been recognized that precise monitoring of the on-orbit performance of these observing systems is key to the ability to differentiate actual climate trends from effects of instrument behavior. Consistent radiometric calibration of the sensors over time and across instruments and platforms is essential.

The visible-wavelength sensors on meteorological satellites typically have not been equipped with on-board calibration capabilities. But the interest in developing CDRs has prompted efforts to develop radiometric calibrations for instruments now long past their operational lifetimes.

This report documents a means to apply radiance calibrations to the visible-channel imagers on a selected group of meteorological satellites, using the Moon as an external radiometric reference. These calibrations are realized by comparing measurements of the lunar brightness derived from satellite images against the reference standard provided by the USGS lunar calibration system. The USGS system predicts the lunar brightness for the specific conditions of the satellite observations with high precision from computations of analytic photometric models of the Moon[1]. The archives of operational meteorological data contain images of the Moon, usually captured by chance. For example, the Moon appears periodically in the off-Earth corners of geostationary satellite images that have a rectangular field of regard, as shown in Figure 1. Because these chance image captures can be relatively infrequent for the GOES 3-hour imaging schedule, NOAA instituted dedicated Moon observations by the GOES-East and West satellites starting in November 2005, with GOES-10.

The Moon embodies a diffuse reflectance source that is exceptionally stable[2]. This property is utilized by the lunar calibration technique to provide a consistent radiometric reference for all sensors that have viewed the Moon, and enables quantitative evaluation of changes in these sensors' response over time. Applied to the instruments in the current study, this effort has produced analytic expressions for converting raw image data to radiances; these expressions are given in the next section.

The information provided in this report is intended for use by CDR developers, to enable the operational datasets from multiple visible-channel imagers to be used together by providing a common, stable radiometric baseline.

[1] H. H. Kieffer and T. C. Stone, The spectral irradiance of the Moon, Astronom. J., 129:2887–2901, (2005)
[2] H. H. Kieffer, Photometric stability of the lunar surface, Icarus, 130:323–327, (1997)

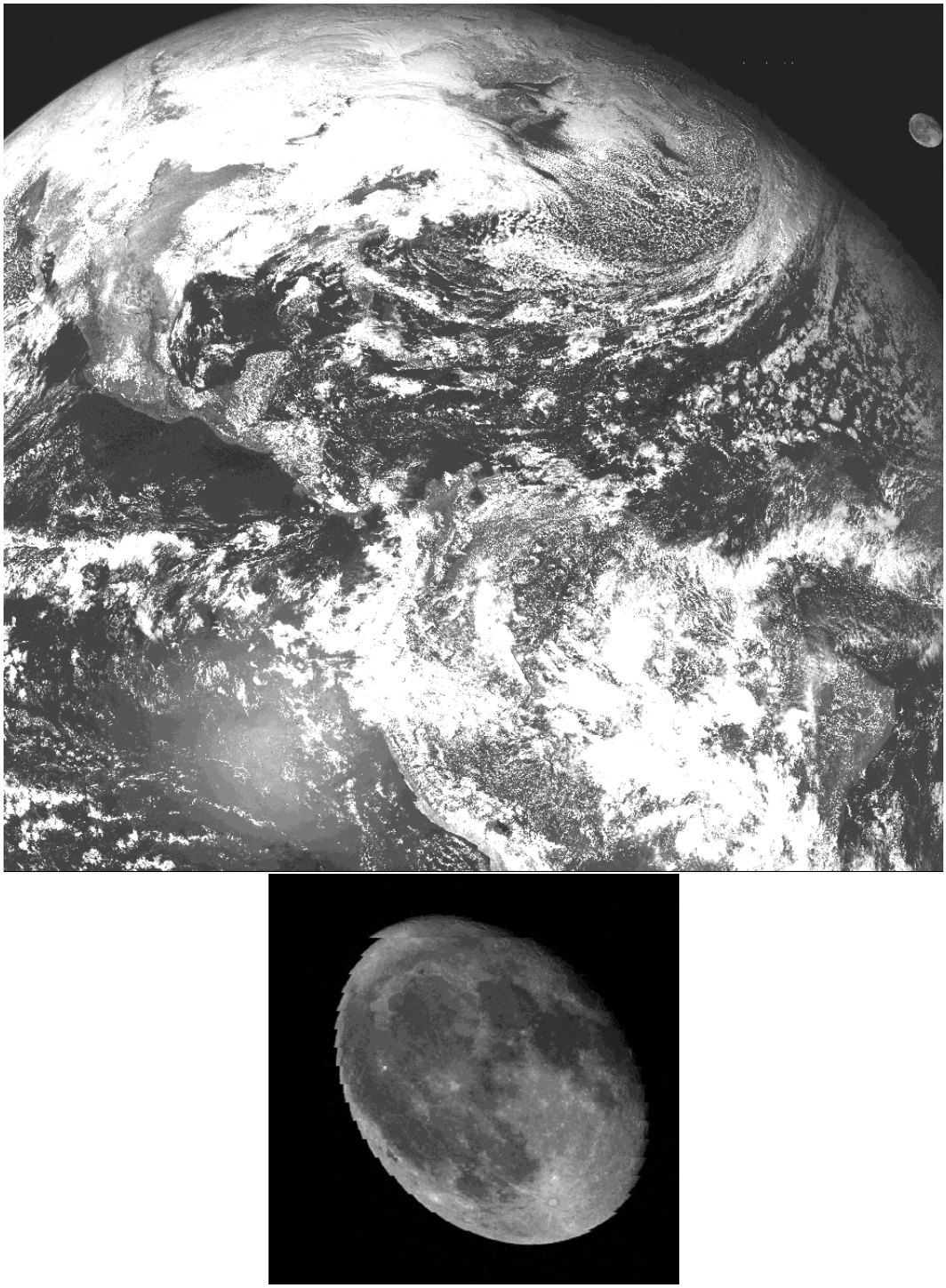

Figure 1: GOES-13 Northern Hemisphere sector image acquired 28 January 2013, 18:45Z, which has captured the Moon in the corner of the field of regard. The close-up of the lunar disk shows the scan line offsets that result from the apparent displacement of the Moon with respect to nadir during image acquisition, induced by the satellite orbital motion.

2 Radiometric Calibrations for Meteorological Imagers

The algebraic expressions and coefficients given in this report provide conversions for raw image data from digital Data Numbers (DN) to spectral radiances in engineering units. They were developed from time series of observations of the Moon acquired by the satellite instruments by comparing measurements of lunar irradiance to the corresponding reference irradiances provided by the USGS lunar calibration system. These time series of radiometric comparisons reveal temporal trends in the sensors' responsivity. The new calibration expressions were formulated to equalize these trends, thus providing temporally stable radiometry for each instrument. The use of a common reference (i.e. the USGS lunar irradiance model, §4.3) for all the satellites provides consistent radiometry among the instruments. The procedures are explained in greater detail and analysis results are presnted in §4 below.

2.1 Calibration Equations

The newly developed calibration expressions have the form of time-dependent corrections to the imager pre-launch coefficients C_0. The time dependence is modeled by a quadratic polynomial function of the elapsed time in days since the specified start time, $(t - t_0)$. The start times have been taken as the operational dates for each satellite. The conversions give per-pixel radiance L_{pix} in Watts/(m^2 sr μm) from the sensor response above the zero-radiance background (i.e. space-view) level, here designated as $(DN - DN_{sp})$. For sensors where the measured radiance is a linear function of sensor response:

$$L_{pix}\left(\frac{\text{Watts}}{\text{m}^2\ \text{sr}\ \mu\text{m}}\right) = C_t(DN - DN_{sp}) \qquad (1)$$

$$C_t = C_0\left[a_0 + a_1(t - t_0) + a_2(t - t_0)^2\right]$$

Satellite	C_0	t_0	a_0	a_1	a_2	$\Delta\lambda_{equiv}$ (μm)
GOES-7*	0.085	05-04-1987	0.933	1.895E-4	0.0	0.2075
GOES-8	0.5502	04-10-1995	1.269	1.755E-4	0.0	0.2013
GOES-9	0.5492	08-07-1995	0.996	5.088E-4	-4.166E-7	0.2177
GOES-10	0.5582	03-21-1998	0.923	3.044E-4	-4.480E-8	0.2175
GOES-11	0.5562	06-21-2006	1.063	1.213E-4	0.0	0.2163
GOES-12	0.5771	04-01-2003	1.036	1.902E-4	-2.657E-8	0.2174
GOES-13	0.6118	04-14-2010	1.098	1.507E-4	-2.904E-8	0.1434
GOES-15	0.5854	12-06-2011	1.141	1.538E-4	0.0	0.1506
Meteosat-8		08-22-2002				
VIS 0.6	0.5537		1.050	1.612E-5	0.0	0.0715
VIS 0.8	0.4496		0.985	1.450E-5	0.0	0.0589
NIR 1.6	0.08703		0.883	2.077E-6	0.0	0.1248
Meteosat-9		12-22-2005				
VIS 0.6	0.4906		1.034	1.636E-5	0.0	0.0700
VIS 0.8	0.3971		0.975	1.560e-5	0.0	0.0582
NIR 1.6	0.08301		0.874	4.055e-6	0.0	0.1234

* Important: VISSR sensors have non-linear response; see §2.4 below

2.2 Background Levels (DN_{sp})

To measure absolute radiances from images, the background level of the data must be corrected to zero. The pixel values of raw image data typically include a small positive bias resulting from a constant voltage applied in the sensor analog signal processing chain during image acquisition. Sensor calibration equations typically specify the background level as an offset or intercept term.

For GOES-8 and the later GOES instruments (often referred to as GVAR) the background level is nominally fixed at $DN_{sp} = 29$ by the space clamp system. The on-board space clamp mechanism evaluates the sensor response to views of deep space, then fixes the bias to give the specified zero-radiance output value. A consequence of this technique is that the actual sensor response to the actual space-view radiance (which may include stars, for example) is lost. The values of space-viewing pixels typically exhibit a normal distribution centered around the clamp setting, and some drifting may occur between space clamp operations.

The pre-GVAR Visible-Infrared Spin-Scan Radiometer (VISSR) instruments on GOES-7 and earlier satellites exhibit large variations in the background levels among the 8 detectors that make up the sensor. Image processing for radiometric measurements requires equalizing the detectors to obtain as close to a uniform zero background level as achievable. Applying this process to all pixels substantially affects the sensor response to the lunar radiance source. This represents a major source of uncertainty in the lunar measurements from the pre-GVAR instruments used in this study.

Image data that have been processed to level-1 already have the background offset corrected to zero. The polynomial of Equation 1 can still be applied to give temporal calibration adjustments to level-1 data, provided the a_0 term is scaled to match the fractional difference in the image calibration from the pre-launch coefficient C_0.

2.3 Spectral Radiance vs. Integrated Radiance

The quantity L_{pix} in Equation 1 gives spectral radiance in Watts/(m^2 sr μm). Some analyses of data from meteorological imaging systems expect pixel values to be expressed as integrated radiances, with units such as Watts/(m^2 sr). The spectral radiances generated by Equation 1 can be converted to integrated radiances by direct multiplication by the sensor band equivalent width in micrometers. These values are given as $\Delta\lambda_{equiv}$ in the coefficients table above.

2.4 Pre-GVAR VISSR Sensors

In the early years of meteorological satellite imagery, it was common practice to accommodate a sensor's full dynamic response range within a smaller numerical output range by applying non-linear transformations in the on-board signal processing. The Visible-Infrared Spin-Scan Radiometer (VISSR) instruments, e.g. on GOES-7 and earlier GOES, produced visible-channel image data as the sensor response squared, with 6-bit data words. The corresponding calibration equation has the form:

$$L_{pix}\left(\frac{\text{Watts}}{m^2\ \text{sr}\ \mu m}\right) = C_t(DN^2 - DN_{sp}{}^2) \qquad (2)$$

The pre-GVAR image data archived in NOAA's Comprehensive Large Array-data Stewardship System (CLASS) are conveniently available in the McIDAS[3] AREA format. The raw image data

[3] http://www.ssec.wisc.edu/mcidas/

in the AREA_VIS files on CLASS have been converted to 8-bit words by bit-wise multiplication by 4, i.e. 2-bit left-shifted.

The coefficients given in the table above for pre-GVAR satellites are intended for use with AREA_VIS 8-bit image data and Equation 2.

2.5 Meteosat SEVIRI Sensors

The calibration expressions and the coefficients in the table of §2.1 for Meteosat-8 and 9 are intended for use with Level-1.5 image data produced by the Spinning Enhanced Visible and InfraRed Imager (SEVIRI) instruments. The Meteosat operating agency, EUMETSAT, specifies conversion of Level-1.5 pixels (in DN) to radiance using a linear transformation of the form:

$$L_{pix} = \text{Cal_Offset} + (\text{Cal_Slope} \times \text{DN}) \tag{3}$$

Using the parameters Cal_Offset and Cal_Slope found in SEVIRI Level-1.5 image headers, this conversion gives spectral radiance in wavenumber units, $\text{mW}/(\text{m}^2\ \text{sr}\ \text{cm}^{-1})$. To compare with results obtained using the calibration expressions developed here, computations using Equation 3 must be converted to equivalent units by multiplication by $10^4/\lambda_{eff}^2$, where λ_{eff} is the effective wavelength of the sensor band in μm, as given below:

	Effective Wavelength (μm)	
band	Meteosat-8	Meteosat-9
VIS 0.6	0.6405	0.6406
VIS 0.8	0.8091	0.8080
NIR 1.6	1.634	1.637

3 AVHRR Lunar Observations

The Advanced Very High Resolution Radiometer (AVHRR) instruments on NOAA polar orbiting satellites periodically capture the Moon by chance in the space-view sector of operational image collects. These encounters can be predicted in advance from a lunar ephemeris and propagating the satellite orbit. The space view sector of AVHRR imagery is used to set the sensor output level for zero radiance input via the space clamp mechanism (cf. §2.2). Intrusions of the Moon severely disrupt the behavior of this system, as it attempts to compensate for the anomalously large sensor response to the scene that is always presumed to be dark. This impacts many scans of AVHRR GAC image data during and after each Moon encounter.

The effect of a Moon intrusion on the AVHRR image background level is shown in Figure 2. This example is illustrative because the lunar disk is fully within the space-view field of regard, but there are two samples in each scan line that contain no lunar radiance, and thus track the background level set by the space clamp system.

The AVHRR space-view sector is 10 pixels wide, with each pixel having an angular acceptance of 1.4 milliradians. The angular size of the lunar disk is 9.04 milliradians at the mean lunar orbital distance, thus AVHRR Moon images frequently are found to be clipped.

To be useful for lunar calibration, the entire lunar disk must be captured in the image, and the lunar radiance must be measured as the sensor response above the background level. The image in

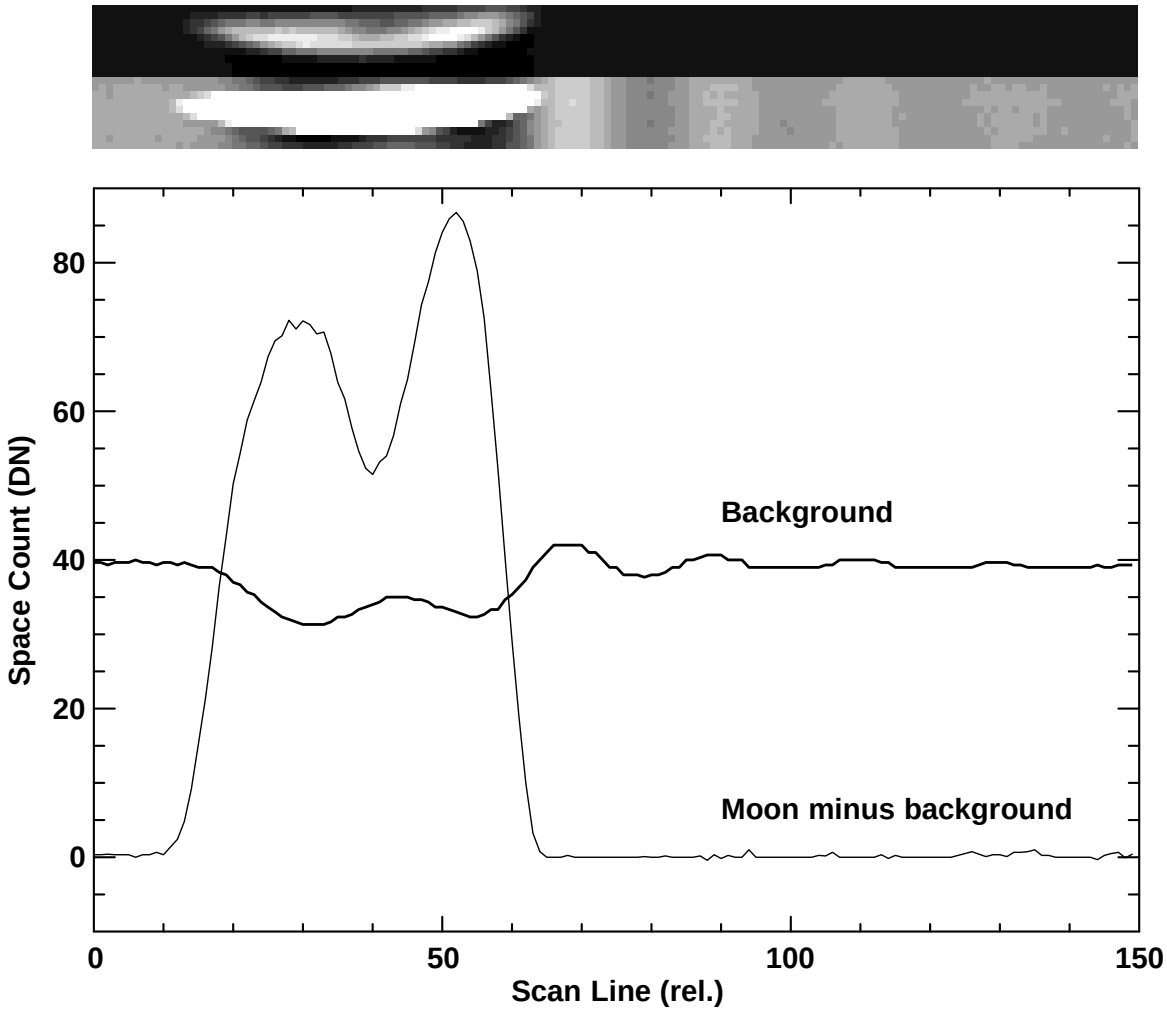

Figure 2: NOAA-16 AVHRR channel 2 (860 nm) image of the Moon captured 12 December 2002, 11:45Z, and plots of mean pixel values. Time increases toward the right. The image is redisplayed stretched to reveal the behavior of the background level, which is set by the space clamp system in response to the intrusion of the Moon. This is shown in the plot labeled "Background", which is an average of the two samples not on the Moon disk (at the bottom of the images). The plot labeled "Moon minus background" is an average of samples on the Moon disk, with the background response subtracted.

Figure 2 is a rare case where the Moon is fully captured and the rapidly varying background level can be evaluated from selected image samples.

The AVHRR space clamp response to the Moon falsely offsets the background level of many scans of GAC data following a lunar intrusion event[4], and the true sensor response to zero radiance is lost. Developing a method to predict this behavior would therefore be useful for AVHRR data analysis in general, in addition to the current image processing for lunar calibration.

The operation of the AVHRR space clamp system likely is described in NOAA and/or instrument manufacturer technical documents, but these are not readily accessible. The temporal behavior of the background level shown in Figure 2 strongly suggests the space clamp works similarly to a Proportional-Integral-Derivative feedback loop controller, such as commonly used for temperature control of building heating and cooling systems. The lunar radiance in AVHRR space-view images can be predicted using the spatially resolved models developed by the USGS Lunar Calibration program, thus the space clamp "error" signal from Moon intrusions can be known. Initial analysis of the NOAA-16 lunar data shows this approach holds promise, but funding limitations of the current CDR project have curbed further efforts. The usefulness for correcting AVHRR image data that have been "contaminated" by lunar intrusions would seem a strong incentive to pursue this line of research.

4 Procedures and Analysis

4.1 Locating Moon Images in the Operational Data Archives

The appearance of the Moon in the space-viewing regions of geostationary imagers can be predicted by computing a lunar ephemeris and propagating the satellite orbit, then finding coincidences of the sensor look direction with the position of the Moon. The prediction algorithm developed for this task simulates the imager scan sequence based on nominal instrument specifications, and checks for coalignment of the Moon position with the scanner look direction for each scan line, within a tolerance to compensate for inaccuracies in the orbit prediction and scan timing, and satellite attitude variations. The lunar phase angle is checked for validity, i.e. within the range of the lunar calibration system.

Predictions of potential Moon captures were found almost exclusively in Full Disk and Northern Hemisphere sector images. After obtaining these data from the NOAA Comprehensive Large Array-data Stewardship System (CLASS), the images were viewed individually to confirm the presence of the Moon. Partial (clipped) Moon images were not used in the analyses.

With the 3-hour scheduling of GOES Full Disk images and the limited space-view margins of other sector coverages, it was found that periods of several months can occur with no by-chance Moon captures at all. This prompted NOAA to institute dedicated observations of the Moon by the GOES-East and West satellites starting in November 2005, with GOES-10. Since then, both the East and West satellites have acquired typically one Moon observation per month through the present (GOES-13 and GOES-15). The CLASS archives were searched for these data, restricting the search criteria to "Routine" operation and "Other" coverages. The dedicated lunar collects usually are indicated as "SPACE" coverage in the CLASS search listings.

[4] A. Ignatov et al., The Usefulness of In-Flight Measurements of Space Count to Improve Calibration of the AVHRR Solar Reflectance Bands, J. Ocean. Atm. Tech., 22:180–200, (2005)

For the GOES imagers, subframes of space-viewing pixels that fully contain the Moon's disk were extracted from the operational images using an interactive selection tool. Ancillary data collected during this process includes the starting sample/line of the subframe with respect to the full frame, and other scan line timing parameters.

Images acquired by the Meteosat Second Generation (MSG) SEVIRI instruments that viewed the Moon were located using an algorithm developed and run at EUMETSAT, which detects the Moon's signature in the IR channel of level-1.0 data. The corresponding solar channel (VIS0.6, VIS0.8 and NIR1.6) images were processed at EUMETSAT, and the lunar image data were made available for the current CDR study. To date, this collection comprises 259 images captured by MSG-1 (Meteosat-8) from November 2003 to March 2012, and 236 images from MSG-2 (Meteosat-9) from July 2006 to December 2012. The SEVIRI instruments on both MSG satellites continue to acquire lunar images during routine operations.

Appearances of the Moon in the AVHRR space-view sector are predicted by computing a lunar ephemeris, then propagating the host satellite orbit and transforming coordinates to the instrument look direction to find coincidences with the Moon position. A small collection of NOAA-16 lunar images has been found in this way, and one with the most favorable conditions was used for the preliminary analysis described in §3 above.

4.2 Lunar Irradiance Measurements from Images

The lunar irradiance E_{Moon} is measured from images by converting pixels to radiance and summing:

$$E_{Moon} = \Omega_{pix} \sum_{i=1}^{N_{pix}} L_i \tag{4}$$

where Ω_{pix} is the angular acceptance (solid angle) of a pixel, L_i is the net radiance value of pixel i, and the sum includes all pixels on the lunar disk N_{pix}. The pixel angular sizes were obtained for each sensor from specifications provided by the satellite operators, and the solid angle is computed as the product of the cross-track size times the down-track size, both in radians.

Although radiance image data have nominally zero background levels, it has been found that consistent lunar irradiance measurements are obtained by selecting and summing only the pixels on the Moon's disk. This was done here with the lunar image subframes as raw data in DN, using an algorithm that specifies a threshold level above the median dark (i.e. true space-view) level and selects pixels above the threshold and within a specified spatial proximity (typically 1 pixel) to the above-threshold pixels. Pixels are then de-selected if they exhibit anomalously high or low values, or if extraneous signal from the Earth limb is detected. The process provides a three-state overlay mask for the image subframes: on-Moon, space, and other pixels.

In this analysis, the designated space pixels were used to evaluate the zero-radiance offset DN_{sp} for conversion to radiance by:

$$L_{pix} = C_0(DN - DN_{sp})$$

For the pre-GVAR data (e.g. GOES-7), the background evaluation was done for the 8 VISSR detectors individually and applied correspondingly in the radiance conversion:

$$L_{pix} = C_0(DN^2 - DN_{sp}^2)$$

In all cases, the pre-launch calibration coefficients C_0 given in §2.1 were applied as constants in the conversions used for the trending analysis (cf. §4.4).

Computing lunar irradiances by Equation 4 necessarily incorporates any oversampling resulting from the image acquisition scheme, i.e. the relation between the sampling rate, the detector IFOV and the scan rate. The oversampling factors used in this study were obtained from the operational specifications for each instrument and platform. The measured irradiances were scaled by these factors for comparison to the lunar reference values, as described in §4.4 below.

4.3 The Reference Lunar Irradiance

The apparent brightness of the Moon varies continuously through its phases, and the non-uniformity and non-Lambertian reflectance of the lunar surface adds complexity to the phase-dependent behavior. To accommodate this, the lunar radiometric reference takes the form of an analytic model that can be computed for any particular set of conditions of an instrument's observations of the Moon. The model used here, developed by the USGS Lunar Calibration program, predicts the lunar spectral irradiance at reflective solar wavelengths, 350 nm to 2450 nm, for phase angles from eclipse ($\sim 1.5^\circ$) to 90° (the lunar quarter phases).

In operation, the USGS lunar irradiance model predicts the spatially integrated disk-equivalent reflectance of the Moon at 32 discrete wavelengths for a given set of geometric inputs. The lunar disk reflectance is governed only by geometry, specifically the phase angle and the particular hemispheres of the Moon that are illuminated and viewed, i.e the lunar librations. The model input parameters are generated for each Moon observation from the spacecraft position at the observation time and the positions of the Sun and Moon computed by a planetary ephemeris program (DE421). The fundamental model outputs, as a disk reflectance spectrum, are convolved with the spectral bandpass function of the sensor and the solar spectral irradiance to give the lunar irradiance at the sensor band wavelength. Corrections are then applied for the $1/r^2$ dependencies on the Sun–Moon and Moon–observer distances.

The final results of computing the lunar model are predicted lunar irradiances at the instrument band wavelengths for the actual physical circumstances of the observations, i.e. the photometric geometry and distances. These quantities can effectively normalize the brightness of the Moon in the observations, thus providing a consistent reference.

4.4 Lunar Irradiance Comparisons and Development of the Calibration Expressions

The plots of Figures 3 and 5 show ratios of the measured lunar irradiances (cf. §4.2) to the corresponding reference irradiances (cf. §4.3) for the series of Moon images found in the operational data archives for this study. Because the measured irradiances were computed using constant (pre-launch) calibration coefficients, these time series reveal the trends in the sensors' radiometric response over time. For demonstration in the figures, each series has been fitted with a function of time to trace the response behavior of the satellite imagers. For the GOES imagers, this is an exponential decay function. The SEVIRI sensors exhibit slow and highly linear degradation behaviors.

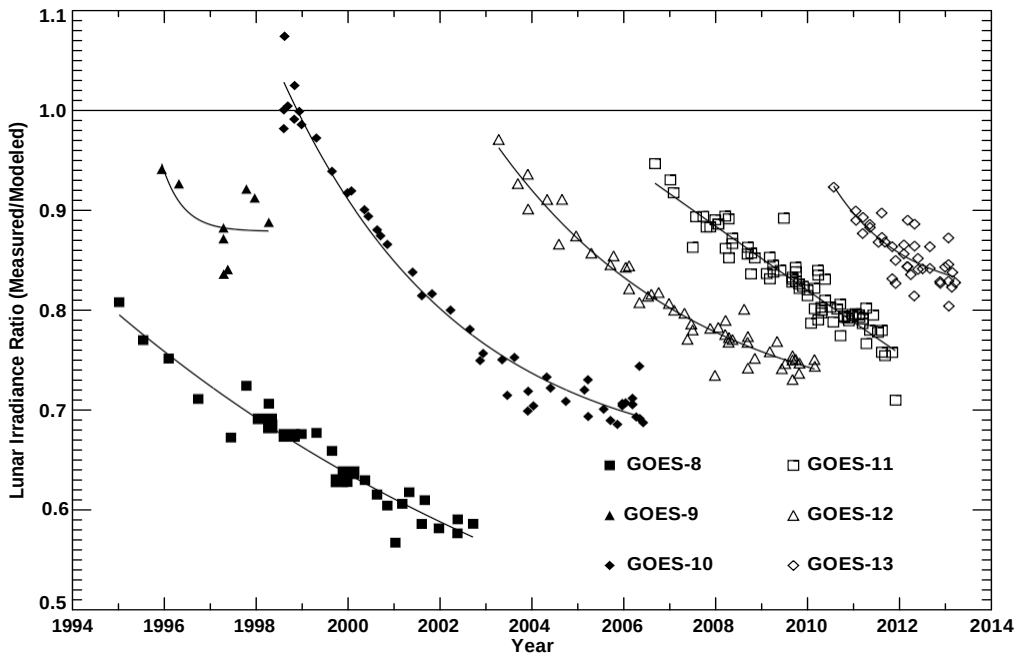

Figure 3: Time series of lunar calibration results for GOES-8 through GOES-13, given as ratios of measured lunar irradiance to lunar model outputs. Trend analysis results are shown as solid lines through the data points.

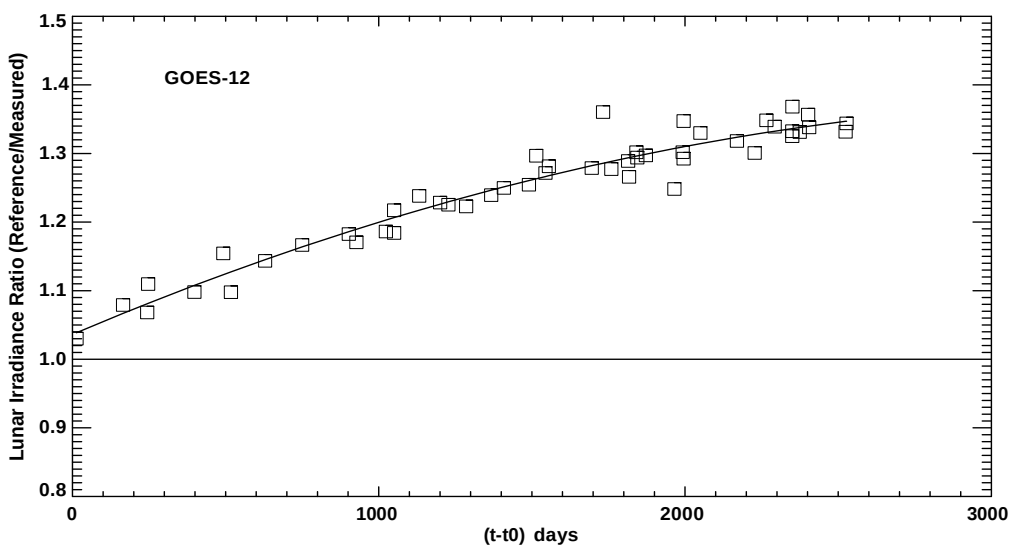

Figure 4: Quadratic temporal fit to the lunar irradiance ratio (reference/measured) for the GOES-12 series. The abscissa is the elapsed time $(t - t_0)$ in days from the satellite operational date. Fits such as this yield the coefficients for Equation 1 given in §2.1.

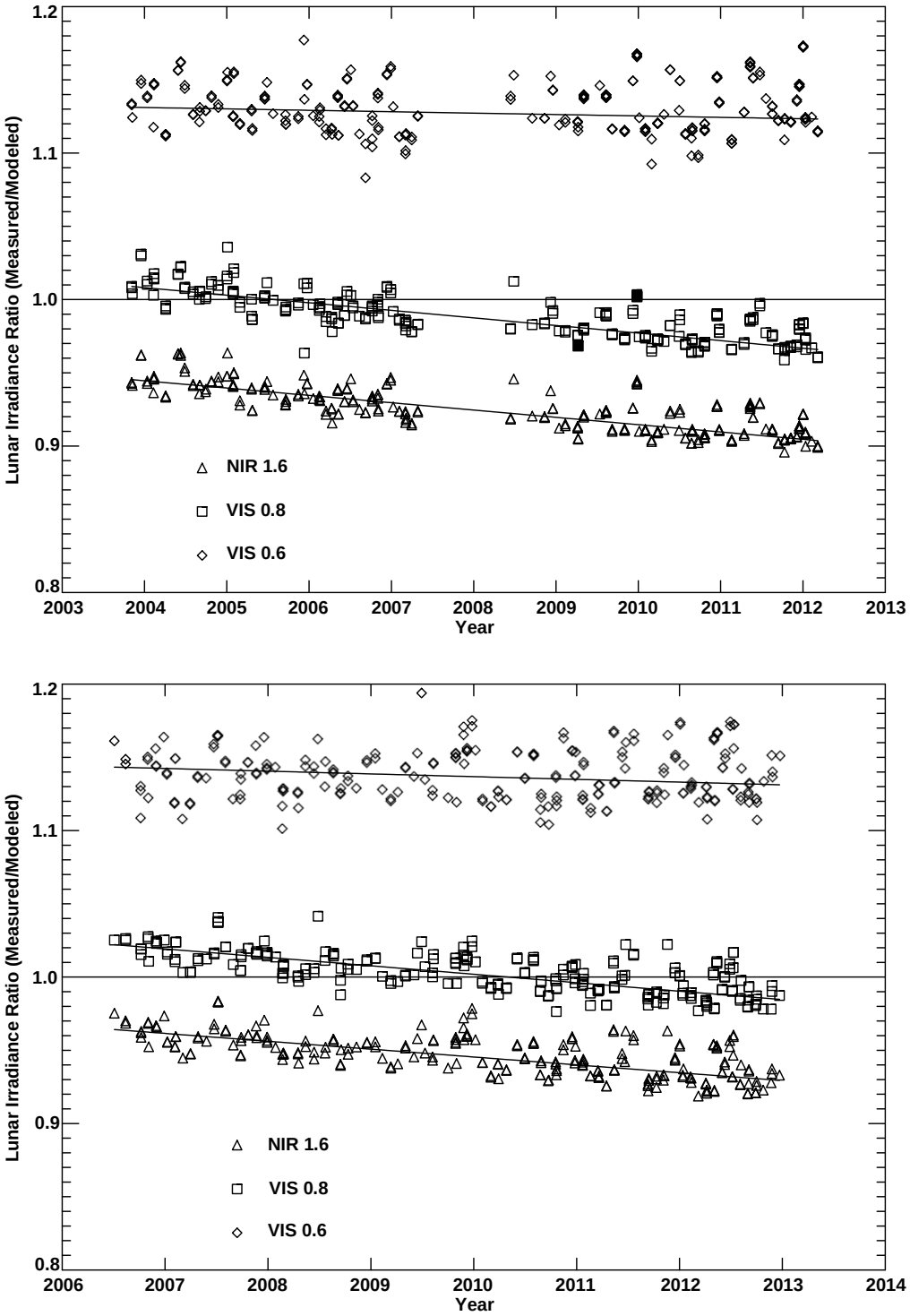

Figure 5: Time series of lunar calibration results for the three SEVIRI solar channels on MSG-1 (top) and MSG-2 (bottom), given as ratios of measured lunar irradiance to lunar model outputs. Trend analysis results are shown as solid lines through the data points.

The driver for development of the calibration expressions given in §2.1 was to produce corrections for the radiometric response of the sensors such that the lunar irradiance measurements agree with the reference irradiances, on average. The quadratic form and coefficients for C_t in Equation 1 were found by fitting the ratio of reference to measured irradiances, E_{ref}/E_{meas}. An example showing the fit for GOES-12 is given in Figure 4.

Figure 6 shows the effect of re-computing the measured lunar irradiances using the time-dependent calibration expressions of §2.1. For clarity, the plot axes are identical to Figure 3. The fitting process determines average trends, and the scatter in the measurements remains in these corrected plots. By developing the corrections using a common reference, provided by the USGS lunar irradiance model, the new calibrations place all the sensors on the same radiometric scale.

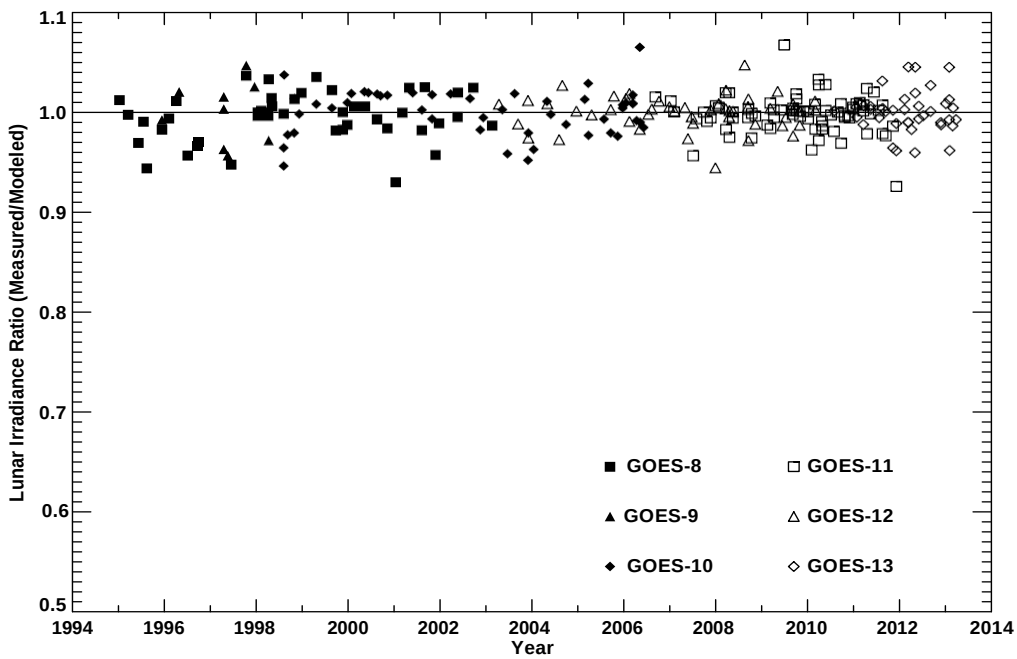

Figure 6: Time series of lunar calibration results for GOES-8 through GOES-13, where the measured irradiances have been re-computed using the time-dependent calibration expressions given in §2.1. The temporal trends have been equalized, and the sensors have been placed on a common radiometric scale.

4.5 Uncertainties

The scatter in the lunar comparison data, seen as e.g. the deviations from the fit line in Figure 4 or from the 1.0 line in Figure 6, give an indication of the uncertainties in the lunar calibrations developed here. The table below gives two measures of the "goodness of fit" of the polynomial fits to the sensor degradation trends, namely the mean absolute deviation $\overline{\text{AbsDev}}$ and the χ^2 parameter:

Satellite	$\overline{\text{AbsDev}}$	χ^2
GOES-7	0.05209	0.4641
GOES-8	0.02654	0.04425
GOES-9	0.02732	0.00871
GOES-10	0.02246	0.03893
GOES-11	0.01508	0.04044
GOES-12	0.01497	0.02137
GOES-13	0.02082	0.03718
GOES-15	0.01430	0.01197
Meteosat-8		
VIS 0.6	0.00847	0.03358
VIS 0.8	0.00793	0.02900
NIR 1.6	0.01107	0.05171
Meteosat-9		
VIS 0.6	0.00964	0.03578
VIS 0.8	0.00805	0.02440
NIR 1.6	0.01086	0.04235

Because the fitted quantities are ratios (of lunar irradiances), the quality parameters given above are fractional values. The mean deviations are generally between 1% and 3% for the GOES imagers (except GOES-7), and close to 1% for the SEVIRI instruments. The magnitude of the χ^2 parameter provides an assessment of how well the polynomial function models the trends. The choice of a linear or quadratic fit was driven by minimizing both these measures, and also by considering the number of data points available for fitting.

The uncertainty in the irradiance comparison data is attributable to uncertainties in both the measurements from images and the reference lunar irradiance computations. The predictions of the USGS lunar model are well-understood, and their relative error over the full valid range of phase angles has been evaluated at under 1%. However, recent analyses of new, high-quality lunar measurements from space-based imagers have suggested a possible residual phase dependence in the model. This is work in progress.

The irradiance measurements from images probably contribute the largest source of error in the comparison data, therefore the measurement processes were examined in detail to assess the associated uncertainties. It was found that the threshold-and-proximity method for selecting pixels on the lunar disk, described in §4.2, produced the most reliable measurements of several techniques tried. However, notable inconsistencies among the measurements remain, regardless of the image processing technique used. This is clearly demonstrated by instances where Moon images were captured in close succession. For example, three lunar images were acquired by GOES-13 within a span of 70 minutes on 28 January 2013. The pertinent observation parameters are given in the table below, and the measured and reference lunar irradiances are visualized in the following figure:

Observation Time 2013-01-28	Operational Imaging	Phase angle (deg)	E-W Nadir angle (deg)	Lunar Irradiance μWatts/(m^2 nm) Measured	Reference	Number of pixels on the lunar disk
17:37:46	Space: Moon	18.24	-8.34	2.18	2.123	113220
17:48:05	Full Disk	18.51	-6.09	2.23	2.107	116560
18:47:09	NH sector	20.08	6.82	2.04	2.034	110120

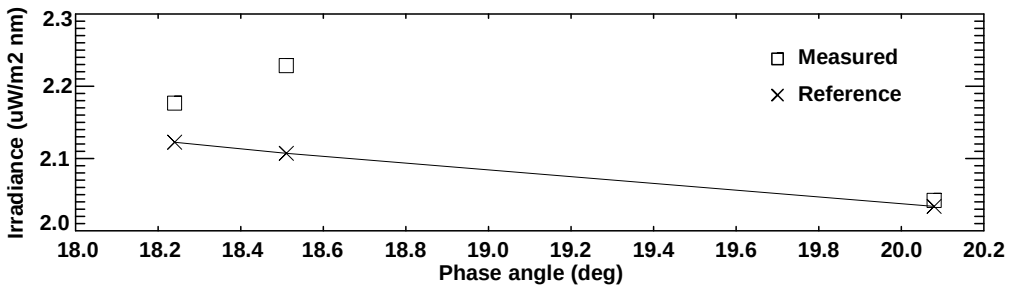

Figure 7: Lunar irradiances for three Moon images acquired within 70 minutes by GOES-13 on 28 January 2013. The phase angle monotonically increases with time, and can be used as a proxy for the East-West nadir angle of the observations.

For this example, the measured lunar irradiances have been generated using the corrected calibration expression of Equation 1. Several potential causes of the observed variations in the lunar radiometry were examined:

Scan mirror angle dependence The current dataset contains a number of instances where lunar observations were acquired in close succession, e.g. with Full Disk and Northern Hemisphere imaging. Typically the Moon appears in opposite corners of the field of regard in these cases. It was found that the differences between the lunar irradiance measurements from the West-side and East-side images were consistently larger than the corresponding changes in the reference irradiance predictions. This strongly suggests an angular dependence of the scan mirror reflectivity.

Oversampling variations The oversampling factor was considered constant for all Moon images acquired by a particular imager. For example, the GOES-I–M and GOES-N–P Databooks specify the oversampling factor to be 1.75 for GOES-8 through GOES-15. In the GOES-13 example above, the increasing phase angle changes the fraction of the illuminated lunar disk by about 0.5%. The number of pixels specified as being on the Moon should closely track this illuminated fraction. The variation in this parameter shown in the table suggest an inconsistency in the oversampling of the images. As a further test, the three consecutive GOES-13 images were corrected for the scan line offsets induced during acquisition (cf. Figure 1), which renders the lunar disk into a nominally elliptical shape. An ellipse was then fitted to the illuminated edge of the disk (the lunar bright limb), as shown in Figure 8 below. The fitted ellipse parameters are:

Observation 2013-01-28	Semi-major axis (pixels)	Semi-minor axis (pixels)	Major/Minor Ratio (oversampling)	Area (pixels)
17:37:46	252.8	146.2	1.729	116074
17:48:05	255.7	148.5	1.722	119262
18:47:09	243.7	144.1	1.692	110309

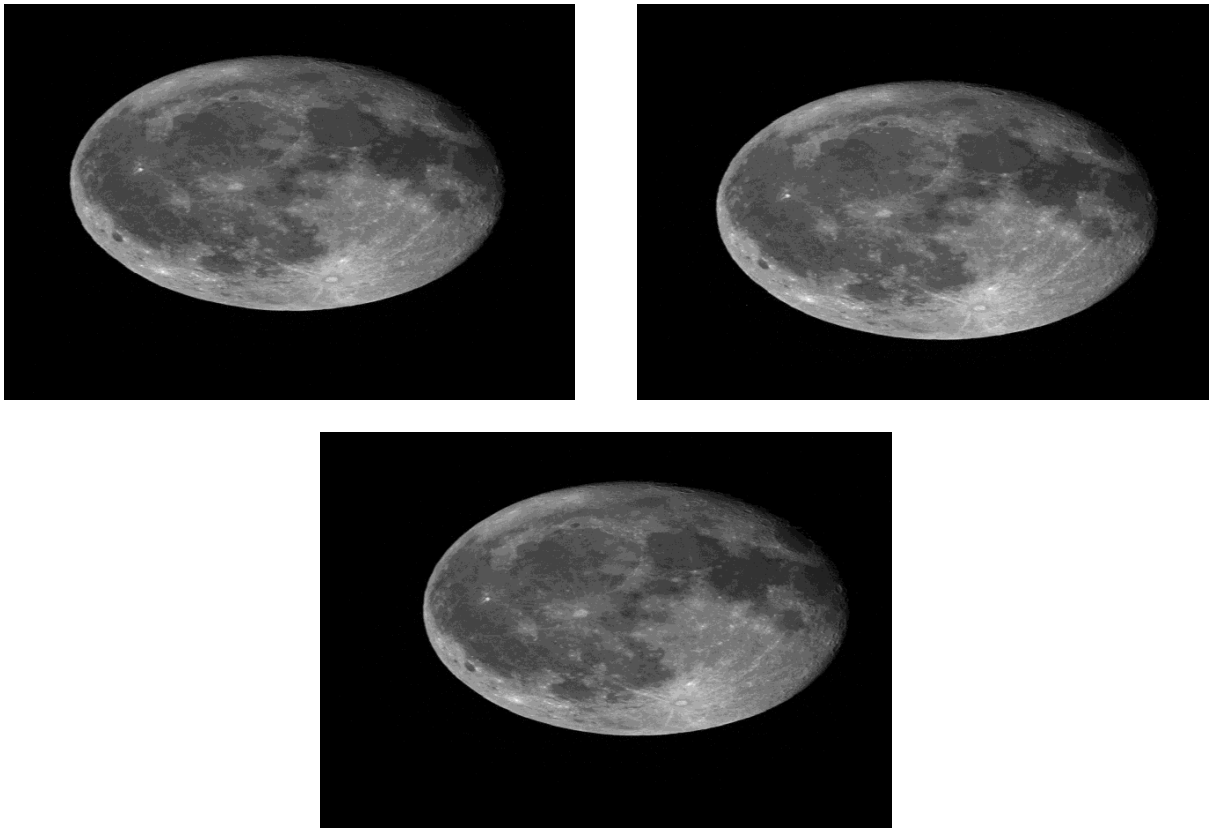

Figure 8: GOES-13 Moon images acquired 28 January 2013, 17:37:46 (top left), 17:48:05 (top right) and 18:47:09 (bottom). The images have been corrected for scan line timing offsets and the bright limb of each has been fitted with an ellipse, shown.

Although the accuracy of the ellipse fitting procedure may be somewhat less than exact, the sizes of the fitted ellipses track the number of on-Moon pixels well. These parameters suggest there are variations in the spatial sampling of the GOES imagers.

Zero-radiance level fluctuations For the GOES visible channel imagers, the values of true space-viewing pixels were found to have normal distributions around the fixed space clamp level. However, the space clamp system as implemented on these instruments sets its fixed value for whatever radiance is measured during the clamp observations. If anomalous signal is present in these radiance measurements, such as from bright stars, the response level of the entire image will be shifted. An extreme example of this effect is shown by intrusions of the Moon in the AVHRR space-view sector, as described in §3 and the reference cited therein. Such offsets in the sensor response will have a strong effect on measurements of the Moon, since the average lunar reflectance is much lower than typical Earth scenes. Because the actual radiance level of the space clamp measurements is not known, the resulting response offsets cannot be evaluated.

5 Conclusions and Recommendations

The analysis reported here has produced time-dependent calibration expressions, which when applied to the specified imager instruments, furnishes stable and consistent radiometry from the

sensors. These calibrations equalize the sensor degradation trends, and place all the sensors on a common radiometric scale. Both properties are essential for CDR development using data products derived from these instruments.

The common radiometric scale specified by this work is provided by the USGS lunar spectral irradiance model. Currently this model is the most reliable reference for lunar radiometry. The Lunar Calibration facility at the USGS Astrogeology Science Center has demonstrated proficiency in using the Moon as a calibration reference for satellite imagers. It is recommended that NOAA consult with USGS for their lunar calibration needs.

The uncertainty analysis conducted for this study has revealed an apparent dependency of the GOES scan mirror angle that affects the radiometry from the visible channel imagers. This circumstance should be investigated further, and if confirmed, the imagers' radiometric calibration equations should include a term related to the nadir view angle. Additionally, the apparent variation in the spatial sampling of GOES images warrants further attention, requiring examination of the satellite telemetry data.

The GOES imagers acquire dedicated observations of the Moon typically once per month. The accuracy of lunar calibrations could be improved by increasing the frequency of these dedicated observations. Also, to characterize the scan mirror angle dependence, additional lunar observations should be acquired which capture the Moon on opposite sides of the field of regard when the opportunities are available. These opportunities can easily be predicted far in advance. An important further recommendation is to acquire the dedicated Moon views with a contiguous scan sequence, uninterrupted by space clamp or star observations.

Intrusions of the Moon in AVHRR space-view acquisitions severely impact the subsequent GAC Earth observation data for hundreds of scans following an event. Quantitative analysis of this effect potentially can lead to development of corrections for the GAC data. This requires knowledge of the lunar radiance sensed by the AVHRR instruments. The USGS Lunar Calibration facility has the database and expertise to conduct such an analysis for NOAA.